Supporting Information:

Porous biscuit-like nanoplates FeNb$_{11}$O$_{29-x}$@C for lithium-ion storage and oxygen evolution

Hongliang Fu [a], Yue Lian [a], Yongqing Bai [a], Zhifeng Wang [b], Yongfeng Hu [c], Jing Zhao [a], Huaihao Zhang [a],*

[a] School of Chemistry & Chemical Engineering, Yangzhou University, Yangzhou 225002, PR China

[b] Testing Center of Yangzhou University, Yangzhou University, Yangzhou 225002, PR China

[c] Department of Chemical Engineering, University of Saskatchewan, Saskatoon, S7N 2V3, Canada

Experimental Section

Synthesis of FeNb$_{11}$O$_{29}$ precursor

FeCl$_3$·6H$_2$O (0.65 mmol) and NbCl$_5$ (7.15 mmol) were dissolved in isopropanol (60 mL) and stirred for 12 h at room temperature. The obtained solution was transferred into a Teflon-lined autoclave (100 mL) and kept at 200 °C for 24 h. After cooling down naturally, the precipitate was collected by centrifugation, washed with deionized water and ethanol individually, and dried at 80 °C for 12 h in a vacuum oven, thus acquiring FeNb$_{11}$O$_{29}$ precursor.

Synthesis of FeNb$_{11}$O$_{29}$ and FeNb$_{11}$O$_{29}$-Piece

(1) The obtained FeNb$_{11}$O$_{29}$ precursor was hold at 900 °C for 4 h in a tubular furnace in N$_2$ atmosphere at a heating rate of 2 °C min^{-1} to form FeNb$_{11}$O$_{29}$ (the contrast sample). (2) The FeNb$_{11}$O$_{29}$ precursor (0.24 g) was dissolved in methanol (20 mL), after which a certain amount of 2-methylimidazole was dissolved in the above solution and stirred for 4 h at room temperature. Then, the precipitate was collected by centrifugation, washed with deionized water and methanol respectively, and dried in a vacuum oven at 80 °C for 12 h. Afterwards, the acquired sample was kept at 900 °C for 4 h in a tubular furnace in N$_2$ atmosphere at a heating rate of 2 °C min^{-1} to obtain the porous biscuit-like nanoplates FeNb$_{11}$O$_{29}$ (named FeNb$_{11}$O$_{29}$-Piece).

Synthesis of FeNb$_{11}$O$_{29-x}$@C

The FeNb$_{11}$O$_{29}$-Piece was subjected to H$_2$ plasma etching (the output power and time of the etching system were 400 W and 20 min, respectively) to afford FeNb$_{11}$O$_{29-x}$-Piece with oxygen vacancies. Then, the FeNb$_{11}$O$_{29-x}$-Piece (0.15 g) was well dispersed in Tris aqueous solution (tris (hydroxymethyl) aminomethane, 100 mL, 10 mmol) with pH 8.5, and later, the dopamine (50 mg) was added to the above solution and polymerized under magnetic stirring for 10 h. After the reaction, the precipitates were collected by centrifugation, washed with deionized water and ethanol, and dried in a vacuum oven at 80 °C for 12 h. Afterwards, the collected sample was calcined at 700 °C for 2 h in a tube furnace under N$_2$ atmosphere to acquire the porous biscuit-like nanoplates FeNb$_{11}$O$_{29-x}$-Piece with carbon layer (named FeNb$_{11}$O$_{29-x}$@C).

OER electrochemical test

The electrochemical measurements were tested using a three-electrode system by Bio-Logic VSP electrochemical workstation (Bio-Logic Co., France) at room temperature (25 °C). Here, the three-electrode system was based on a glassy carbon electrode (GCE, diameter: 3 mm, area: 0.07 cm^2) as the working electrode, and graphite rods and Hg/HgO electrodes as the counter electrode and reference electrode, respectively. The potential reported in this work was converted from $E_{(RHE)} = E_{(Hg/HgO)}$ + 0.0591×pH + 0.098 V to reversible hydrogen electrode (RHE). The catalyst overpotential was calculated using the equation: $\eta_{(V)} = E_{(RHE)} - E^{\theta}$, where E^{θ} represents OER thermodynamic potential (1.23 V vs. RHE).

Preparation of working electrode

The as-obtained catalysts (5 mg) were uniformly dispersed in the mixed solution of 950 μL absolute ethyl alcohol and 50 μL Nafion solution (5 wt%), and then 5 μL catalysts ink was dropped on the surface of the glassy carbon electrode.

Before conducting electrochemical experiments, the electrolyte was purified with pure nitrogen for 30 min, and then the newly prepared working electrode was immersed in the electrolyte. The cyclic voltammetric curves were obtained by scanning the electrode Hg/HgO in the voltage range of 0-0.7 V at room temperature (scan rate: 5 mV s^{-1}). Then Tafel plots were recorded by LSV curves at a scan rate of 5 mV s^{-1}.

Tafel slope analysis

The overpotential values are defined by the Tafel equation: $\eta = a + b\log|j|$, where $\eta_{(V)}$ is the overpotential, j (mA cm^{-2}) is the current density, b(mV dec^{-1}) represents the Tafel slope.

ECSA calculation and measurement

The electrochemical surface area (ECSA) was evaluated by double layer capacitance (C_{dl} in mF): ECSA = C_{dl}/C_s

The ECSA was determined by cyclic voltammetry (CV) from 0.79 V to 0.99 V in 1 mol/L KOH at scan rate 20, 40, 60, 80 and 100 mV s^{-1}. The C_{dl} was ascertained by fitting the slope of $\triangle j = (j\text{a} - j\text{c})/2$ at 0.89 V vs. RHE and various scan rate. The specific capacitance is available for a flat surface by assuming 40 μF cm^{-2} (C_s). The ECSA was achieved by normalizing the double layer capacitance to a standard specific

capacitance.

Specific activity and Turnover frequency (TOF)

The specific activity was obtained by normalizing the apparent current to ECSA. Specific activity was calculated as follows: Specific activity = $j{\times}A$/ECSA, where j is the current density, A is the surface area, ECSA is the electrochemical surface area of the catalyst.

The TOF value is calculated by the formula:

$$TOF = \frac{j * A}{4 * F * m}$$

where j is the current density at a particular potential, A is the electrode surface area, F is the Faraday constant (96485 C mol^{-1}), and m is the mole number of active substance.

Electrochemical Impedance Spectroscopy (EIS) analysis

The EIS was recorded at the frequency range from 1000 kHz to 10 mHz with 10 points per decade. The amplitude of the sinusoidal potential signal was 5 mV.

Stability test and Chronoamperometry (CA) measurement

The dynamical stability was tested for 5000 cycles at the constant scan rate of 150 mV s^{-1}. The polarization curve was compared with the initial curve to assess catalyst stability after 5000 cycles. Meanwhile, to further estimate catalyst stability, the CA was performed at a potential 1.52 V vs. RHE for OER in 1mol L^{-1} KOH solution for 10 h.

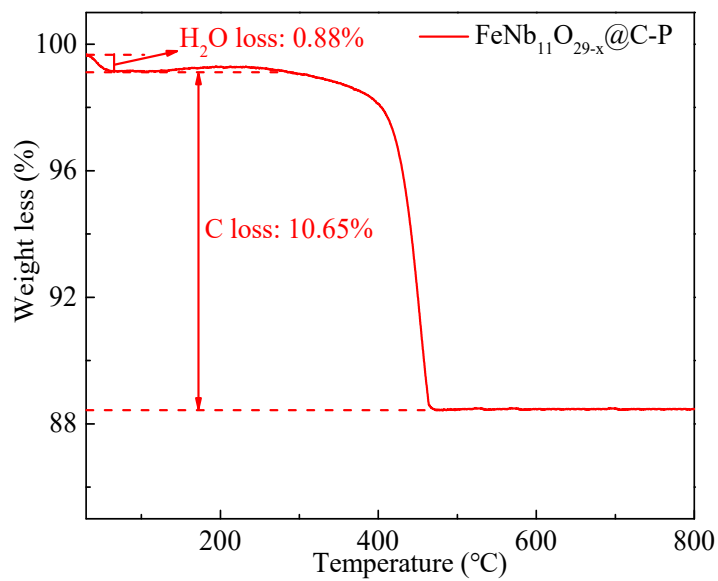Figure. S1 TGA curve of FeNb$_{11}$O$_{29-x}$@C

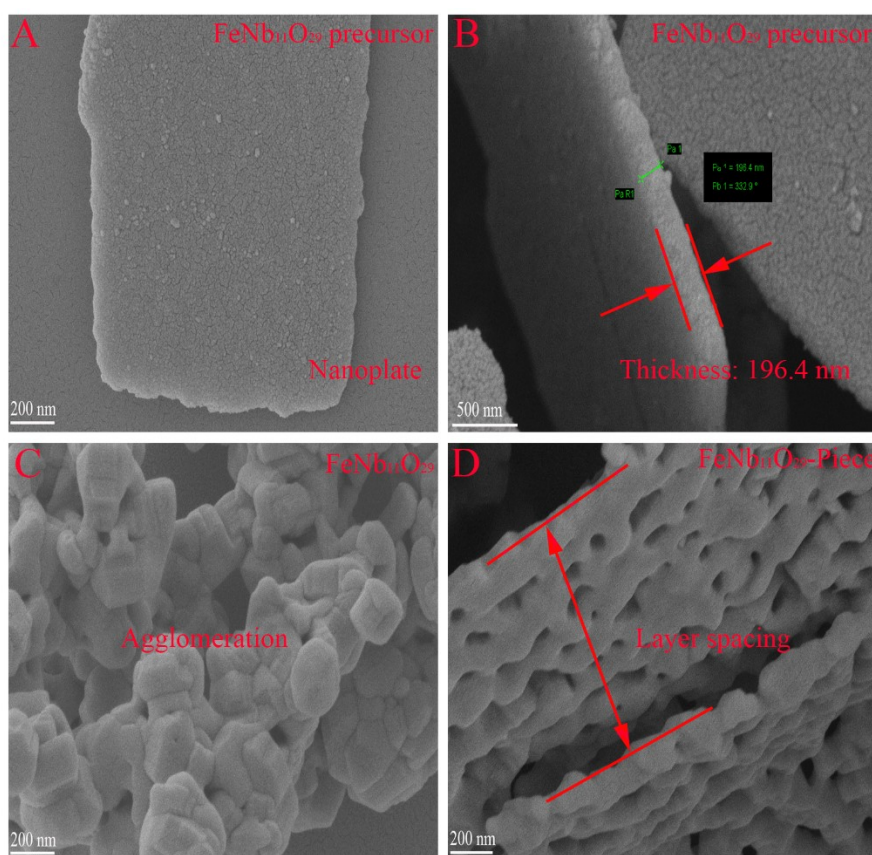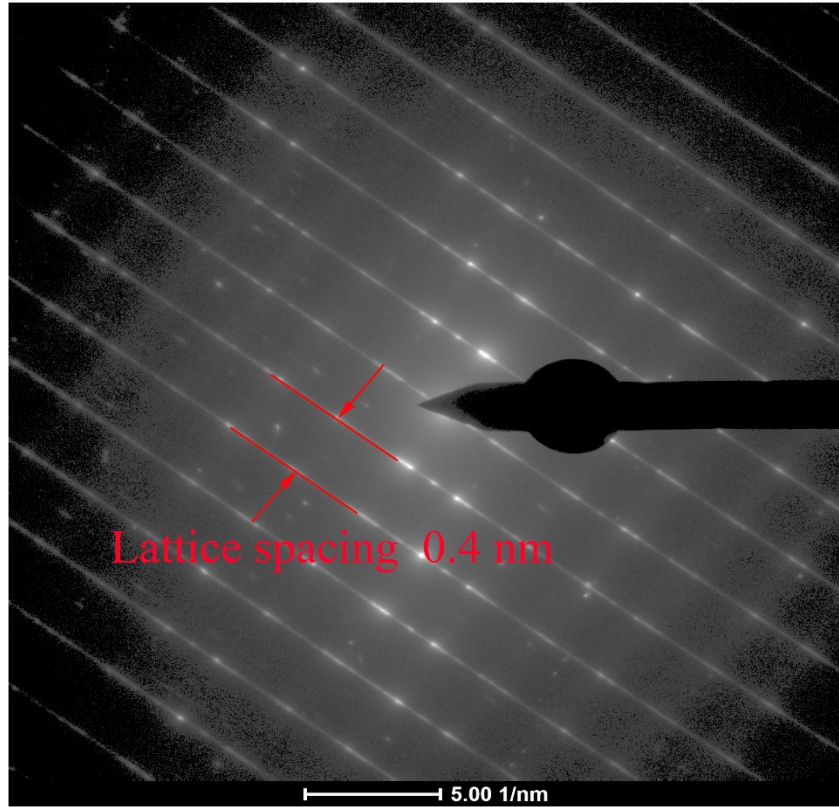Figure. S2 SEM of FeNb$_{11}$O$_{29}$ precursor (A and B), FeNb$_{11}$O$_{29}$ (C) and FeNb$_{11}$O$_{29}$-Piece (D).
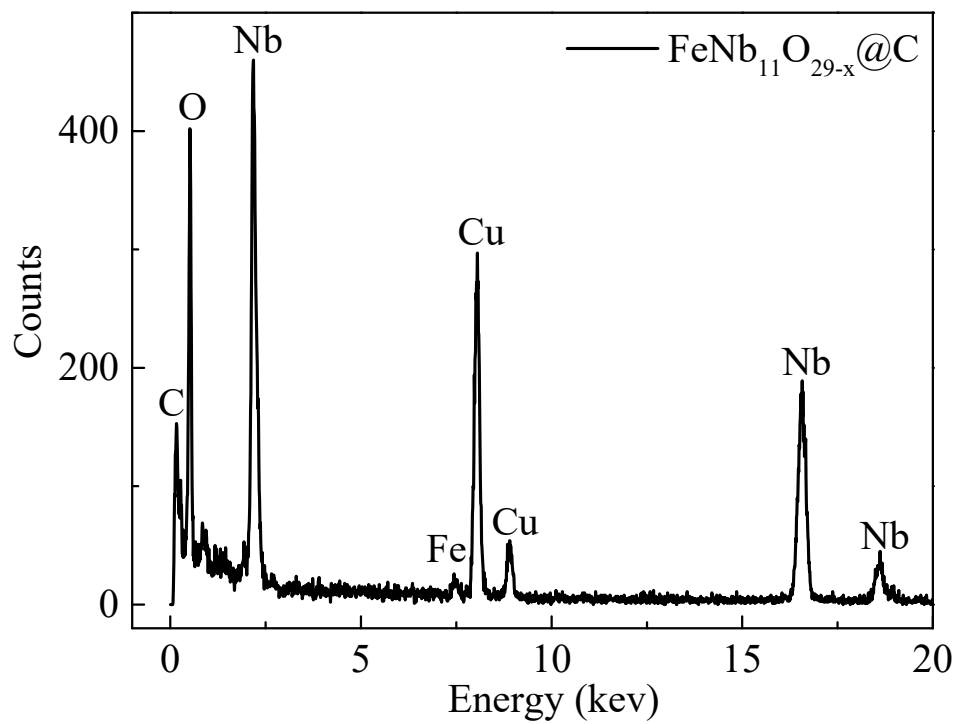
Figure. S3 SAED pattern of FeNb$_{11}$O$_{29-x}$@C.

Figure. S4 EDS of FeNb$_{11}$O$_{29-x}$@C. (Copper element from the TEM matrix)

Table. S1 BET parameters of samples.

Sample	S_{BET} (m^2 g^{-1})	V_{micro} (cm^3 g^{-1})	S_{micro} (m^2 g^{-1})	D_m (nm)	Average Particle Size (nm)
FeNb$_{11}$O$_{29}$	4.9	0.0012	2.3	6.2	1126.3
FeNb$_{11}$O$_{29}$-Piece	20.4	0.0063	4.7	6.9	766.1
FeNb$_{11}$O$_{29-x}$@C	48.1	0.013	7.6	8.8	748.8

S_{BET}: BET surface area.

V_{micro}: micropore volume.

S_{micro}: mesopore surface area.

D_m: average pore diameter.

Table. S2 Quantification results from EDS

Element	Weight (%)	Atomic (%)	Uncertainty (%)	Correction	k-Factor
C (K)	4.95	15.56	0.36	0.26	4.032
O (K)	22.01	54.26	0.46	0.49	2.008
Fe (K)	2.86	1.32	0.04	0.99	1.359
Nb (K)	69.16	28.84	0.98	0.99	3.705
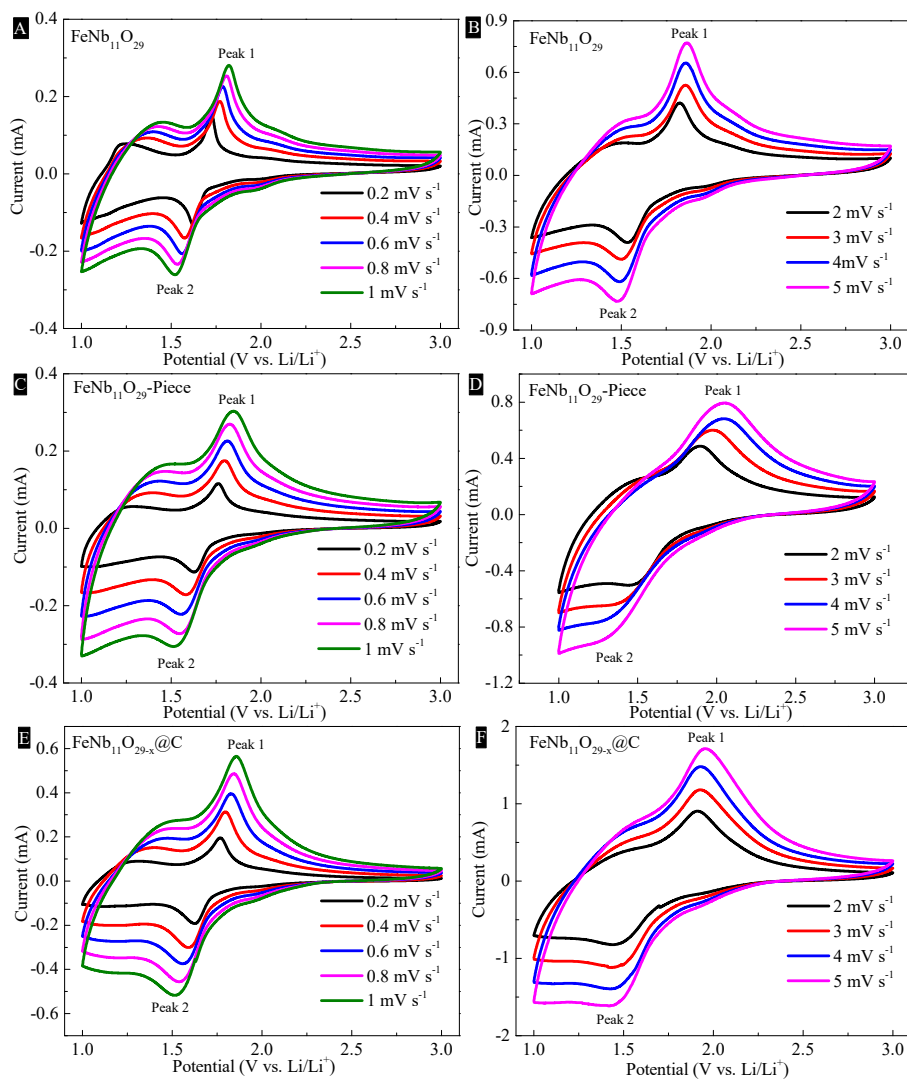
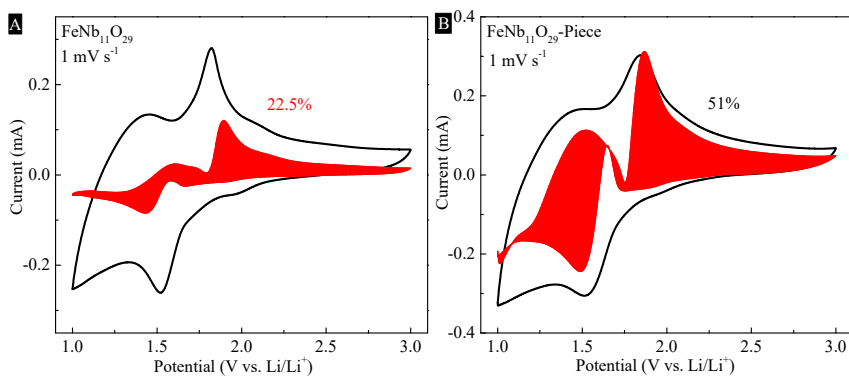Figure. S5 CV curve of FeNb$_{11}$O$_{29}$ (A, B), FeNb$_{11}$O$_{29}$-Piece (C, D) and FeNb$_{11}$O$_{29-x}$@C (E, F) at different sweep rate.

Figure. S6 Separation of the total current (solid line) and capacitive currents (shaded regions) at 1.0 mV s^{-1} of FeNb$_{11}$O$_{29}$ (A) and FeNb$_{11}$O$_{29}$-Piece (B).
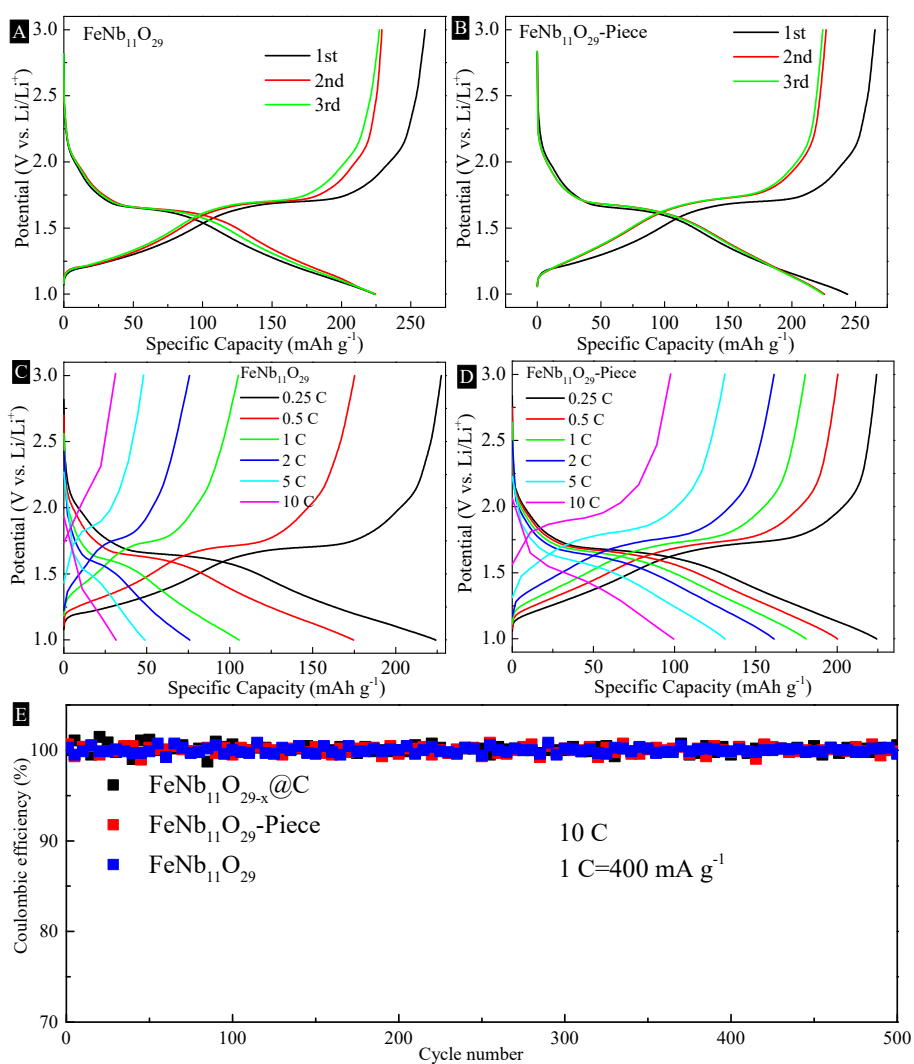
Figure. S7 GCD curves of FeNb$_{11}$O$_{29}$ (A, C) and FeNb$_{11}$O$_{29}$-P (B and D); (E) Coulombic efficiency of FeNb$_{11}$O$_{29}$, FeNb$_{11}$O$_{29}$-Piece and FeNb$_{11}$O$_{29-x}$@C at 10 C.
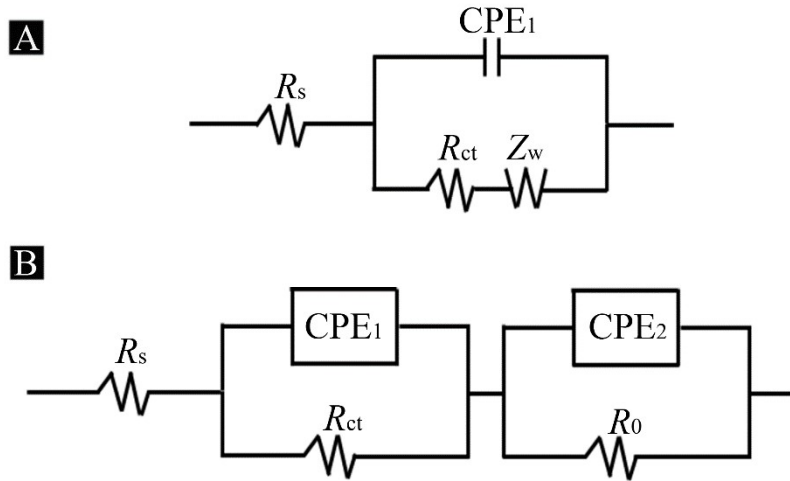
Figure. S8 Circuit diagram used for the EIS data fitting of LIB (A) and OER (B).

Table S3. EIS fitting parameters from the equivalent circuits for different samples (LIB).

Samples	R_s/Ω	R_{ct}/Ω	Z_w/Ω	CPE_1/Ω
$FeNb_{11}O_{29}$	10.1	236.9	6.7E-3	5.6E-6
$FeNb_{11}O_{29}$-Piece	10.6	110.7	1.3E-2	1.5E-6
$FeNb_{11}O_{29-x}@C$	9.7	57.6	9.7E-3	4.4E-6

Table S4. EIS fitting parameters from the equivalent circuits for different samples (OER).

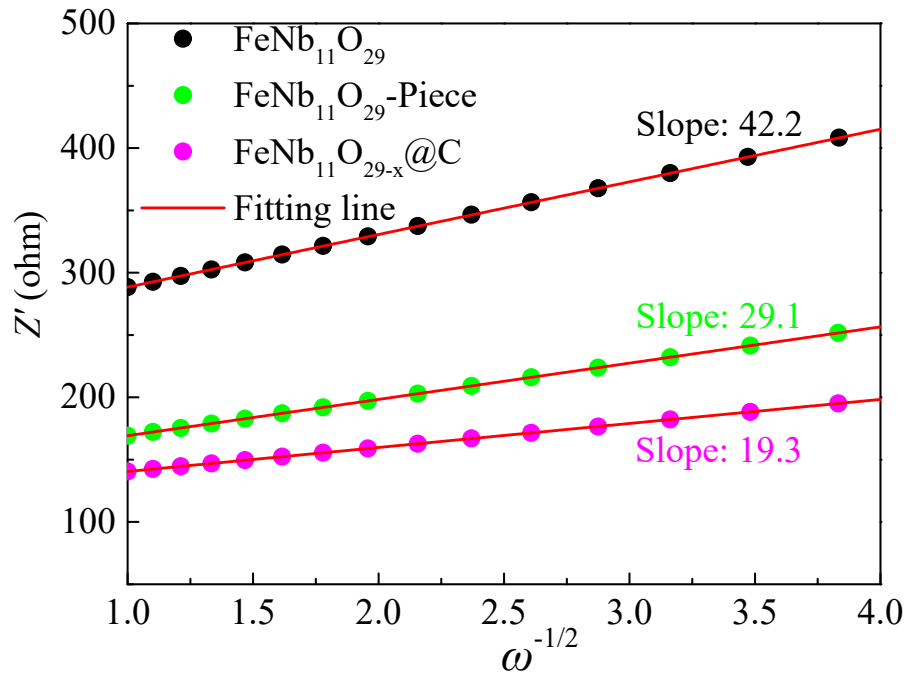| Catalysts	R_s/Ω	R_{ct}/Ω	R_0/Ω	CPE_1/Ω	CPE_2/Ω
$FeNb_{11}O_{29}$	9.1	469	8.3	2.6E-3	1.5E-5
$FeNb_{11}O_{29}$-Piece	7.9	227.6	12.2	7.8E-5	2.3E-3
$FeNb_{11}O_{29-x}@C$	8.2	105.2	2.7	2.3E-4	3.3E-2

Figure. S9 Warburg impedance coefficient (σ) from the linear fitting line of Z' versus $\omega^{-1/2}$.
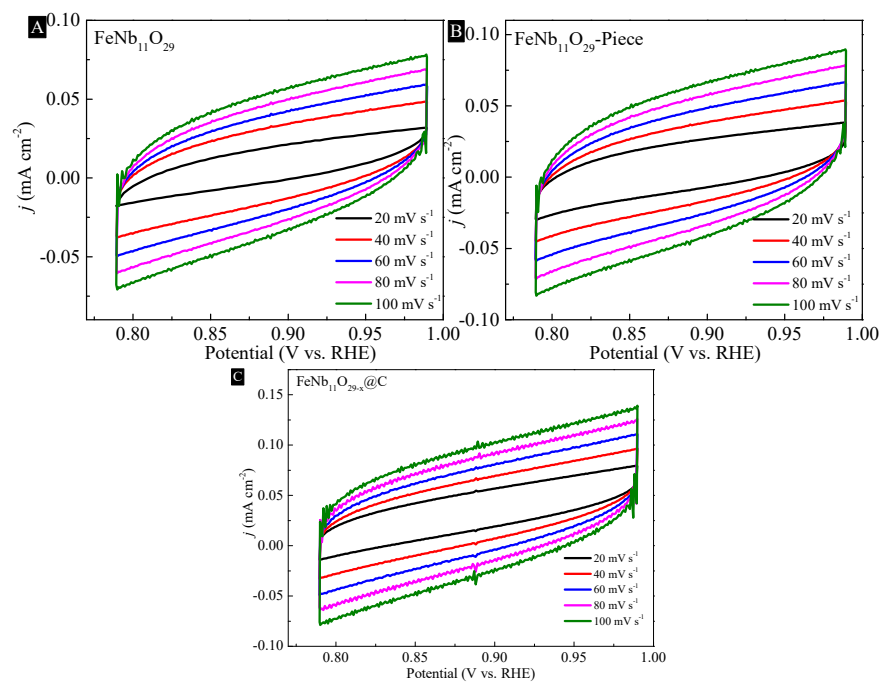
Figure. S10 Cyclic Voltammograms of $FeNb_{11}O_{29}$ (A), $FeNb_{11}O_{29}$-Piece (B) and $FeNb_{11}O_{29-x}@C$ (C).
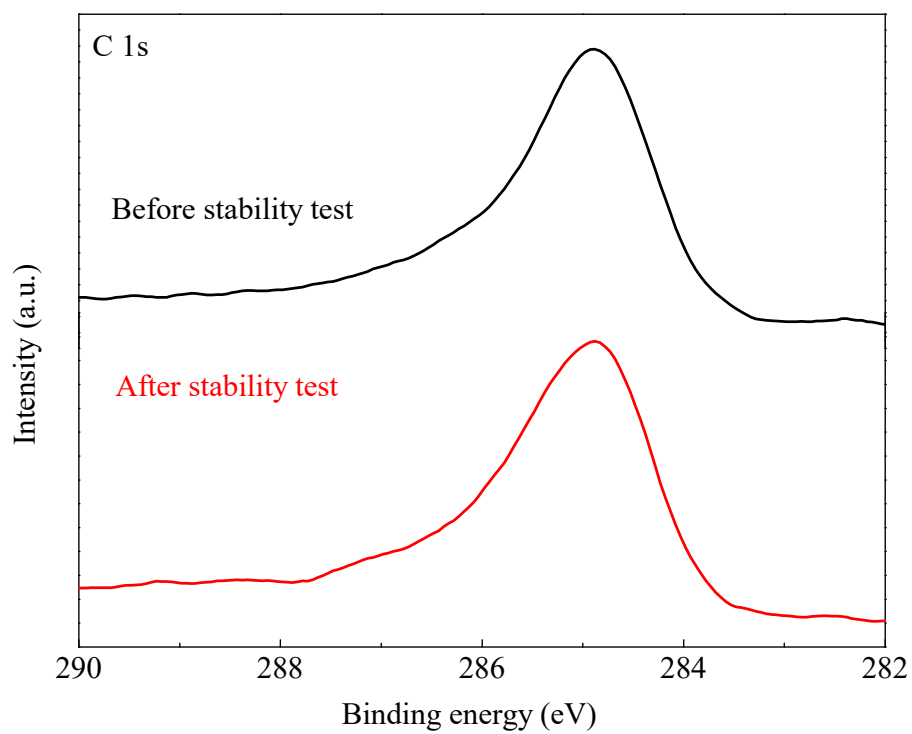
Figure. S11 C 1s XPS spectra of FeNb$_{11}$O$_{29-x}$@C before and after stability test.

Table. S5 Lithium electrical properties of niobium based bimetallic oxides.

Sample	Capacitance	Cyclic performance	References
$FeNb_{11}O_{29-x}$@C	240.8 mAh g^{-1} @ 0.25 C	99.02% after 500 @ 10 C	This work
$FeNb_{11}O_{29}$ nanotubes	233.2 mAh g^{-1} @ 1 C	69.8% after 2000 @ 10 C	[1]
$Cr_{0.2}Fe_{0.8}Nb_{11}O_{29}$	254 mAh g^{-1} @ 0.1 C	86.9% after 500 @ 10 C	[2]
$CrNb_{11}O_{29}$-P	235 mAh g^{-1} @ 0.5 C	90.2% after 400 @ 10C	[3]
$AlNb_{11}O_{29}$-M	225 mAh g^{-1} @ 1 C	93.2% after 500 @ 10C	[4]
$Ti_2Nb_{11}O_{29}$	234 mAh g^{-1} @ 1 C	46% after 500 @ 10C	[5]
$GaNb_{11}O_{29}$@C	226.8 mAh g^{-1} @ 0.1 A g^{-1}	99.64% after 500 @ 0.1 A g^{-1}	[6]
S-$TiNb_2O_7$	231 mAh g^{-1} @ 0.1 A g^{-1}	72.9% after 300 @ 0.1 A g^{-1}	[7]
S-$V_3Nb_{17}O_{50}$@NC	222.1 mAh g^{-1} @ 0.1A g^{-1}	86.2% after 2000 @ 0.5 A g^{-1}	[8]
$Mg_2Nb_{34}O_{87}$-M	253 mAh g^{-1} @ 0.5 C	93.5% after 500 @ 10C	[9]
$Zn_2Nb_{34}O_{87}$-B	241 mAh g^{-1} @ 0.5 C	86.8% after 1000 @ 10C	[10]
$Cu_2Nb_{34}O_{87}$	239.4 mAh g^{-1} @ 1 C	99.83% after 300 @ 1C	[11]
M-$MoNb_{12}O_{33}$	215 mAh g^{-1} @ 1 C	89.2% after 1000 @ 10C	[12]
$ZrNb_{14}O_{37}$ nanowires	236.4 mAh g^{-1} @ 0.1A g^{-1}	99.97% after 1000 @ 0.1 A g^{-1}	[13]
$HfNb_{24}O_{62}$	223 mAh g^{-1} @ 0.5 C	87.1% after 500 @ 10C	[14]

Table. S6 Comparison of Fe/Nb-based OER electrocatalysts in alkaline electrolyte.

Catalysts	Electrolyte	Current density (mA cm^{-2})	Overpotential (mV)	References
FeNb$_{11}$O$_{29-x}$@C	1M KOH	10	290	This work
FeNb$_{11}$O$_{29}$-Piece	1M KOH	10	337	This work
FeNb$_{11}$O$_{29}$	1M KOH	10	391	This work
NiFeNb$_4$-OH	1M KOH	10	306	[15]
Fe$_{90}$Nb$_{10}$	1M KOH	10	340	[16]
Nb-Ni$_3$N	1M KOH	10	380	[17]
Nb CNF-Pt	1M KOH	10	325	[18]
CaMn$_{0.75}$Nb$_{0.25}$O$_{3-x}$	1M KOH	10	550	[19]
Co, Nb-MoS$_2$/TiO$_2$ HSs	1M KOH	10	340	[20]
NbFe-Ni$_x$Se$_y$	1M KOH	50	470	[21]
Fe-Mo/Te-2	1M KOH	10	300	[22]
BaZr$_{0.15}$Fe$_{0.85}$O$_{3-\delta}$	1M KOH	10	412	[23]
Ni$_{1.12}$Fe$_{0.49}$Se$_2$	1M KOH	10	227	[24]
Fe/Ni-CoTe@NCFs	1M KOH	10	287	[25]
Co2-Fe-B	1M KOH	10	298	[26]
Ni/Fe/CP	1M KOH	10	300	[27]
FeCo-N-C-700	1M KOH	10	370	[28]

Table. S7 Change in the peak positions of Fe and Nb elements Before and after OER test.

Elements / OER test	Fe		Nb	
	Fe $2p_{3/2}$	Fe $2p_{1/2}$	Nb $3d_{5/2}$	Nb $3d_{3/2}$
Before OER test	711.9 eV	725.5 eV	207.6 eV	210.3 eV
After OER test	712.2 eV	725.9 eV	207.7 eV	210.5 eV

Table. S8 Fe and Nb concentrations by ICP

Sample / Element	Fe	Nb
$FeNb_{11}O_{29-x}@C$	0.0316 mmol L^{-1}	0.342 mmol L^{-1}
$FeNb_{11}O_{29}$-Piece	0.0323 mmol L^{-1}	0.352 mmol L^{-1}

References:

1   R. Zheng, S. Qian, X. Cheng, H. Yu, N. Peng, T. Liu, J. Zhang, M. Xia, H. Zhu and J. Shu, *Nano Energy*, 2019, **58**, 399–409.

2   X. Lou, Z. Xu, Z. Luo, C. Lin, C. Yang, H. Zhao, P. Zheng, J. Li, N. Wang, Y. Chen and H. Wu, *Electrochim. Acta*, 2017, **245**, 482–488.

3   Q. Fu, X. Liu, J. Hou, Y. Pu, C. Lin, L. Yang, X. Zhu, L. Hu, S. Lin, L. Luo and Y. Chen, *J. Power Sources*, 2018, **397**, 231–239.

4   X. Lou, R. Li, X. Zhu, L. Luo, Y. Chen, C. Lin, H. Li and X. S. Zhao, *ACS Appl. Mater. Interfaces*, 2019, **11**, 6089–6096.

5   W. Mao, K. Liu, G. Guo, G. Liu, K. Bao, J. Guo, M. Hu, W. Wang, B. Li, K. Zhang and Y. Qian, *Electrochim. Acta*, 2017, **253**, 396–402.

6   Z. Wang, R. Zheng, Y. Li, H. Yu, J. Zhang, X. Zhang, W. Bi, M. Shui and J. Shu, *Ceram. Int.*, 2020, **46**, 5913–5919.

7   Y. Zhang, M. Zhang, Y. Liu, H. Zhu, L. Wang, Y. Liu, M. Xue, B. Li and X. Tao, *Electrochim. Acta*, 2020, **330**, 135299.

8   H. Fu, Q. Duan, Y. Lian, D. Wang, Y. Bai, Z. Cao, J. Sun, J. Zhao and H. Zhang, *Chem. Commun.*, 2022, **58**, 6080–6083.

9   X. Zhu, Q. Fu, L. Tang, C. Lin, J. Xu, G. Liang, R. Li, L. Luo and Y. Chen, *ACS Appl. Mater. Interfaces*, 2018, **10**, 23711–23720.

10   X. Zhu, H. Cao, R. Li, Q. Fu, G. Liang, Y. Chen, L. Luo, C. Lin and X. S. Zhao, *J. Mater. Chem. A*, 2019, **7**, 25537–25547.

11   X. Cai, H. Yan, Z. Yang, J. Zhang, H. Yu, L. Zhang and J. Shu, *Ceram. Int.*, 2021, **47**, 24511–24518.

12   X. Zhu, J. Xu, Y. Luo, Q. Fu, G. Liang, L. Luo, Y. Chen, C. Lin and X. S. Zhao, *J. Mater. Chem. A*, 2019, **7**, 6522–6532.

13   Y. Li, R. Zheng, H. Yu, X. Cheng, T. Liu, N. Peng, J. Zhang, M. Shui and J. Shu, *ACS Appl. Mater. Interfaces*, 2019, **11**, 22429–22438.

14   Q. Fu, H. Cao, G. Liang, L. Luo, Y. Chen, V. Murugadoss, S. Wu, T. Ding, C. Lin and Z. Guo, *Chem. Commun.*, 2020, **56**, 619–622.

15   J. Pan, S. Hao, X. Zhang and R. Huang, *Inorg. Chem. Front.*, 2020, **7**, 3465–3474.

16   C. Wang, R. Wang, Y. Peng, J. Chen, Z. Chen, H. Yin and J. Li, *J. Mater. Chem. A*, 2020, **8**, 24598–24607.

17   J. Xiang, W. Zou and H. Tang, *Catal. Sci. Technol.*, 2021, **11**, 6455–6461.

18   S. Shanmugapriya, P. Zhu, C. Yan, A. M. Asiri, X. Zhang and R. K. Selvan, *Adv. Mater. Interfaces*, 2019, **6**, 1900565.

19   Y.-Q. Lyu and F. Ciucci, *ACS Appl. Mater. Interfaces*, 2017, **9**, 35829–35836.

20   D. C. Nguyen, T. L. Luyen Doan, S. Prabhakaran, D. T. Tran, D. H. Kim, J. H. Lee and N. H. Kim, *Nano Energy*, 2021, **82**, 105750.

21   Y. Qiu, Z. Liu, X. Zhang, A. Sun, X. Ji and J. Liu, *J. Colloid Interface Sci.*, 2022, **610**, 194–201.

22   R. He, M. Li, W. Qiao and L. Feng, *Chem. Eng. J.*, 2021, **423**, 130168.

23   K. Zhu, H. Liu, X. Li, Q. Li, J. Wang, X. Zhu and W. Yang, *Electrochim. Acta*, 2017, **241**, 433–439.

24   Y. Du, G. Cheng and W. Luo, *Nanoscale*, 2017, **9**, 6821–6825.

25   W. Li, J. Chen, Y. Zhang, W. Gong, M. Sun, Y. Wang, X. Wang, H. Rao, J. Ye and Z. Lu, *Int. J. Hydrogen Energy*, 2021, **46**, 39912–39920.

26   H. Chen, S. Ouyang, M. Zhao, Y. Li and J. Ye, *ACS Appl. Mater. Interfaces*, 2017, **9**, 40333–40343.

27   Z. Xu, R. Fan, X. Zhou, G. Huang, X. Wu and M. Shen, *ACS Sustain. Chem. Eng.*, 2019, **7**, 19832–19838.

28   X. Duan, S. Ren, N. Pan, M. Zhang and H. Zheng, *J. Mater. Chem. A*, 2020, **8**, 9355–9363.